Supplement of Atmos. Chem. Phys., 24, 8569–8587, 2024
https://doi.org/10.5194/acp-24-8569-2024-supplement

Atmospheric Chemistry and Physics
Open Access

Supplement of

Concentration and source changes of nitrous acid (HONO) during the COVID-19 lockdown in Beijing

Yusheng Zhang et al.

Correspondence to: Weigang Wang (wangwg@iccas.ac.cn) and Yongchun Liu (liuyc@buct.edu.cn)

S1. De-weather model

Changes in atmospheric pollutant concentration are affected by emissions and meteorology. Machine learning models, including boosted regression trees and random forest (RF) algorithms, often exhibit higher predictive accuracy because of their advantages in modeling complex relationships between response variables and predictor variables (Zhan et al., 2018). By reducing the variance/bias and error of high-dimensional data sets, it has better performance compared to traditional statistical and air quality models. The algorithm resolves the relationship between air pollutant levels and their predictors, including meteorological parameters and time variables such as the day of the year (Julian Day), day of the week (Monday to Sunday), and hour of the day (0-23) (Grange et al., 2018). The input data set was randomly divided into a training data set for building the RF model (i.e., 70% of the input data set) and a testing data set (30% of the input data set) for testing the performance of the RF model using unseen data sets. The RF model is an ensemble model composed of many individual decision tree models (Breiman, 2001).

In the RF model, the bagging algorithm is utilized, which involves randomly selecting samples from the training dataset, with replacement, along with their respective predictor features. Each decision tree is grown based on various decision rules that optimize the fitting between observed pollutant concentrations (response variable) and their predictor features. The selection of predictor features for each tree node is performed randomly to achieve the best possible split. The predicted pollutant concentrations are determined by aggregating the outcomes of all individual decision trees through a weighted average. The bagging process, by averaging predictions from bootstrap samples, helps reduce variance and mitigates overfitting issues in the model. As shown in Figure S1, the entire data set is randomly divided into two groups, one is the training data set, used to build the random forest model; the other is the test data set, used for testing without seeing the data set. The training data set accounts for 70% of the total data, and the rest is test data. Grange et al. (2018) built the RF model using the R “normalweather” package.

In our study, the parameters of the RF model are as follows: hourly concentrations of HONO, NO, NO_2, O_3, $PM_{2.5}$, SO_2, and CO as dependent variables, meteorological parameters (wind direction, wind speed, air temperature, humidity, and atmospheric pressure) and Time predictors (weekdays, hours) served as independent predictors. The training set uses randomly selected 70% of the data, and the remaining 30% is used as the test set. Random forest models were developed using the rmweather R package (Grange et al., 2018; Grange and Carslaw, 2019). The number of trees is 300, and the number of variables split in each node is 3. For each weather normalization, the explanatory variables are resampled (excluding the time variable) without replacement and randomly assigned to the dependent variable observations. The 1000 predicted values are then aggregated using the arithmetic mean to obtain the deweathered concentration.

Model performance evaluation

Evaluation metrics for the model can be found in Table S5. The random forest model showed good performance in predicting the data compared to the observations in the training and test datasets. Specifically, the R values range from 0.93-0.98. These extremely high correlation values indicate a strong relationship between the predicted values and the observed values, indicating that the characteristics of the established model are excellent. The FAC2 of each indicator is very small, indicating that our model meets the conditions for predicting scores. Likewise, lower NMB and NMGE values indicate that our model performs well. Through the verification of various indicators, it is believed that the model has good prediction ability.

S2. Monte Carlo algorithm

The Monte Carlo algorithm is a method of estimating numerical values through random sampling. It can be used to estimate the overall uncertainty of the numerical value. A large number of samples are generated by random sampling from a probability distribution and the required numerical indicators are calculated based on these samples. Due to the limited number of samples, there is a certain error between the estimated value and the true value. We increase the number of sampling times to 10,000 to reduce

statistical uncertainty.

When establishing the simulation model, the respective change ranges of the variables that affect HONO intensity are input, and the uncertainty of the modeling is evaluated by sampling from the probability distribution of the parameters to obtain the overall uncertainty. In addition, the uncertainty of the model parameters is propagated to the model output through Monte Carlo sampling, and the uncertainty distribution of the results can be obtained. The formula for overall uncertainty can be expressed as:

$$\sigma = \sqrt{\frac{1}{N}\sum_{i=1}^{N}(x_i - \bar{x})^2}$$

σ represents the standard deviation of the overall uncertainty; N is the number of samples; x_i is the value of the i^{th} sample, and $\bar{x}$ is the mean of the sample.

Table S1. Summary of HONO observation sites and source contributions

Location (References)	Date	Measurement area	Site situation	Source contribution
Antarctica (Bond et al., 2023)	2022.01	Research Station	Clean area, covered with ice and snow	Photolysis of nitrate in snow is very important, and its contribution is 10 times greater than the reaction between NO and OH.
Shenzhen (Tang et al., 2024)	2019.10	natural ecological area	Along the coast, there are fewer human activities and more vegetation around it.	Photolysis of large amounts of nitrate in coarse particles completely compensates for unknown sources during the daytime (66%).
China (Xing et al., 2023)	2018.05	sea edge	coastal	In inland areas, the NO_2 heterogeneous reaction on the ground is more important; in coastal and ocean cases, the contribution of aerosol surfaces is greater.
Idaho (Chai et al., 2021)	2018.08	wildfire zone	Smoke collected near five wildfires	In the aging smoke during the daytime, the heterogeneous conversion of NO_2 reaches 85%, followed by NO+OH.
Guangzhou (Li et al., 2012)	2006.07	rural area	Close to farmland, low traffic emissions	The main source at night is NO+OH and the heterogeneous conversion of NO_2 on the ground, and traffic can be ignored
Cyprus (Meusel et al., 2018)	2016.04	rural area	Along the coast, a lot of vegetation is exposed	Emissions from soil and biological soil crusts are important.
Melpitz (Ren et al., 2020)	2018.04	rural area	Nearby are meadows, agricultural areas, and forests	Nocturnal HONO: Heterogeneous conversion of ground NO_2 dominates, and traffic emission is a secondary source.
Wangdu (Liu et al., 2019b)	2014.06	rural area	Intensive agricultural activities and no traffic emissions	Noonday HONO: Soil emissions account for 80%.
Wangdu (Xue et al., 2020)	2017.12	rural area	No traffic emissions, surrounded by farmland	Noonday HONO: The heterogeneous conversion of NO_2 on the ground is 36%, NO+OH is 34%, and the others can be

				ignored.
Wangdu (Song et al., 2022)	2020.06-2020.09	rural area	No traffic emissions, surrounded by farmland	Noonday HONO: The heterogeneous conversion of NO_2 on the ground is dominant (43-62%), followed by NO+OH 12-38%, and the rest are less than 5%.
Wangdu (Zhang et al., 2023)	2020.09-2021.08	rural area	Seriously affected by agriculture and animal husbandry	Direct emissions from rural areas, including animal husbandry, account for 39-45% and cannot be ignored.
Hongkong (Zhang et al., 2016)	2011.08	suburbs	Near the airport, surrounded by vegetation and close to the South China Sea	The heterogeneous conversion of NO_2 on the ground is 42%, soil emission is 29%, marine source is 9%, NO+OH is 6%, aerosol surface conversion is 3%, and traffic is 2%.
Hongkong (Xu et al., 2015)	2011.08-2012.05	suburbs	Areas near airports and highways are mostly covered by vegetation.	Nocturnal HONO: Traffic dominates in the first half of the night (59%), and the heterogeneous conversion of NO_2 on the ground dominates in the second half of the night.
Heshan (Fu et al., 2019)	2017.01	suburbs	Lots of vegetation and farmland, with some scattered villages	Heterogeneous conversion of NO_2 is 72%, traffic is 8%, and NO+OH is 3%. Noonday HONO: Photolysis of nitrate accounts for more than 50%.
Taizhou (Ye et al., 2023)	2018.06	suburbs	Borders farmland and fish ponds	Noonday HONO: The heterogeneous conversion of NO_2 on the ground is 71%, followed by NO+OH, traffic, and aerosol surface conversion. Nocturnal HONO: Heterogeneous conversion of NO_2 on the ground is dominant (55%).
Beijing (Tong et al., 2015)	2014.11	urban area	Densely populated and busy with traffic	Nocturnal HONO: Traffic emission is 40%, NO+OH is 42%, and others are 18%.
		suburbs	By the lake, with farmland nearby	Nocturnal HONO: Traffic emission is 8%, NO+OH is 11%,

				and others are 81%。
Beijing (Tong et al., 2016)	2014.12	urban area	Densely populated and busy with traffic	Nocturnal HONO: Traffic emission is dominant (49%), and the reaction of NO and OH is also important.
		suburbs	By the lake, with farmland nearby	Nocturnal HONO: Heterogeneous conversion of NO_2 is the main source, and traffic is 10%.
Beijing (Zhang et al., 2019a)	2006.08	urban area	Mixed residential, commercial, and transportation area	Nocturnal HONO: Traffic is 41%, ground heterogeneous conversion is 27%, and aerosol surface conversion is 20%. Noonday HONO: ground heterogeneous conversion is 66%, and aerosol surface conversion is 19%.
Beijing (Zhang et al., 2019c)	2016.12	urban area	Densely populated and busy with traffic	Nocturnal HONO: Traffic emission is dominant, reaching 52%, and heterogeneous conversion is not an important pathway.
Beijing (Meng et al., 2020)	2016.12	urban area	Mixed residential, commercial, and transportation area, 325m vertical observation.	High altitude during haze: HONO is dominated by heterogeneous conversion on the aerosol surface; Near the ground: Heterogeneous conversion of NO_2 on the ground is dominant, followed by traffic, accounting for 29%
Beijing (Gu et al., 2021)	2017.05	urban area	Mixed residential, commercial, and transportation area	Noonday HONO: The light-induced heterogeneous transformation of NO_2 on the ground is dominant, and aerosol surface conversion can be ignored.
	2018.01			Noonday HONO: NO+OH is dominant.
Beijing (Liu et al., 2020b)	2018.02-2018.07	urban area	Mixed residential, commercial, and transportation area	Nocturnal HONO: Traffic emission is dominant, reaching 50%, and heterogeneous conversion is not an important pathway. Noonday HONO: Nitrate photolysis and NO+OH are important.

Beijing (Zhang et al., 2020)	2018.04	urban area	Mixed residential, commercial, and transportation area, 325m vertical observation.	At different altitudes, the heterogeneous conversion of NO_2 is the most important source, accounting for more than 70%. Among them, the aerosol surface is dominant.
Beijing (Jia et al., 2020)	2018.08	urban area	Mixed residential, commercial, and transportation area	Traffic is 18%, NO+OH is 31% (clean) and 7% (haze), and the aerosol surface conversion can reach up to 88%, which is very low on the ground. Nitrate photolysis is 15%,
Beijing (Liu et al., 2021)	2018.06 2018.12	urban area	Mixed residential, commercial, and transportation area	Noonday HONO: NO+OH is 22%, traffic is 19%, and Heterogeneous conversion on the aerosol surface is 19%。 Noonday HONO: Heterogeneous conversion on the aerosol surface is 30%, Heterogeneous conversion on the ground is 25%, and traffic is 20%.
Beijing (Zhang et al., 2022)	2019.01	urban area	Densely populated and busy with traffic	Traffic is 28%, Heterogeneous conversion on the ground is 27%, and aerosol surface conversion is 15%。
Beijing (Li et al., 2021)	2019.06	urban area	Mixed residential, commercial, and transportation area	Nocturnal HONO: The heterogeneous conversion of NO_2 is the main pathway, followed by NO+OH. Traffic is 30%.
Shijiazhuang (Liu et al., 2020a)	2019.12-2020.03	urban area	mixed traffic and residential area	Nocturnal HONO: The heterogeneous conversion of NO_2 on the ground is dominant, followed by aerosol surface conversion.
Beijing-Tianjin-Hebei (Zhang et al., 2019b)	2017.12	urban area	Less traffic emissions and intensive agricultural activities	Nocturnal HONO: Traffic and heterogeneous conversion of NO_2 are the main sources.
Xi'an	2015.08	urban area	Mixed residential, commercial,	Nocturnal HONO: The heterogeneous conversion of NO_2 is

(Huang et al., 2017)			and transportation area	the main pathway, followed by NO+OH. Traffic is 19%.
Shanghai (Cui et al., 2018)	2016.05	urban area	Mixed residential, commercial, and transportation area	Nocturnal HONO: Heterogeneous conversion of NO_2 is the main source.
Nanjing (Zheng et al., 2020)	2015.12	urban area	To the west of the steel plant and petrochemical refinery, 15 kilometers from the city center	The heterogeneous conversion of NO_2 is dominant, accounting for 50%, and traffic is 11%.
Nanjing (Liu et al., 2019a)	2017.11-2018.11	urban area	Mixed residential, commercial, and transportation area	Traffic is 23%, heterogeneous conversion on the ground is 36%, Soil emissions can reach 40% in July and August. The aerosol surface conversion reaches 40% (severe haze periods).
Changzhou (Shi et al., 2020)	2017.04	urban area	Mainly residential and commercial areas, with no roads and industrial activities,	Nocturnal HONO: Heterogeneous conversion of NO_2 is 54%, traffic is 32%, and NO+OH is 14%. Noonday HONO: Nitrate photolysis is important.
Guangzhou (Yu et al., 2022)	2018.10	urban area	mixed traffic and residential area	Nocturnal HONO: The three main sources are the heterogeneous conversion of NO_2 on the ground, traffic, and NO+OH. The aerosol surface conversion and soil emissions are not important.
Birmingham (Kramer et al., 2020)	2016.11	urban area	road tunnel	Traffic is dominant, accounting for 66% (up to 86%), the heterogeneous conversion of NO_2 is only 5%,

Table S2. Instruments used in the measurement.

Parameter	Instrument	Time resolution	Detection limit	Accuracy
HONO	LOPAP	60 s	0.01 ppb	10%
NO	Thermo Scientific 42i	60 s	0.05 ppb	5%
NO_2	Thermo Scientific 42i	60 s	0.05 ppb	5%
SO_2	Thermo Scientific 43i	60 s	0.12 ppb	5%
CO	Thermo Scientific 48i	60 s	40 ppb	5%
O_3	Thermo Scientific 49i	60 s	0.5 ppb	5%
$PM_{2.5}$	TEOM	300 s	0.05 μg m^{-3}	10%
Temperature	AWS310	60 s	-	1%
Relative humidity	AWS310	60 s	-	1%
Wind speed	AWS310	60 s	0.01 m s^{-1}	1%
Wind direction	AWS310	60 s	-	1%
UVB	AWS310	60 s	0.001 W m^{-2}	1%
J_{NO2}	2-pi-J_{NO2} radiometer	60 s	1.0×10^{-5} s^{-1}	11% (Shetter et al., 2003)
Boundary layer height	Ceilometer (CL51)	60 s	50 m	10%
Nitrate	ToF-ACSM	600 s	0.021 μg m^{-3}	5%
Sulfate	ToF-ACSM	600 s	0.018 μg m^{-3}	5%
Chloride	ToF-ACSM	600 s	0.011 μg m^{-3}	5%
Ammonium	ToF-ACSM	600 s	0.182 μg m^{-3}	5%
Organic	ToF-ACSM	600 s	0.198 μg m^{-3}	5%

Table S3. Sensitivity analysis with different parameters for the HONO budget

Method	Emission factor	OH	γ_{NO2} (ground)	γ_{NO2} (aerosol)	J_{NO3^-}	*As*	δ	$F_{HONO,soil}$	V_d	$K_{dilution}$	Sensitivity
M0	0.0109	CaV1[a]	2×10^{-6}	2×10^{-6}	8.24×10^{-5}	CaV2[b]	3.85	CaV3[c]	0.001	0.23	-
M1	0.008	CaV1	2×10^{-6}	2×10^{-6}	8.24×10^{-5}	CaV2	3.85	CaV3	0.001	0.23	-8%
M2	0.0186	CaV1	2×10^{-6}	2×10^{-6}	8.24×10^{-5}	CaV2	3.85	CaV3	0.001	0.23	20%
M3	0.0109	CaV1×0.1	2×10^{-6}	2×10^{-6}	8.24×10^{-5}	CaV2	3.85	CaV3	0.001	0.23	-24%
M4	0.0109	CaV1×2	2×10^{-6}	2×10^{-6}	8.24×10^{-5}	CaV2	3.85	CaV3	0.001	0.23	26%
M5	0.0109	CaV1	1×10^{-5}	2×10^{-6}	8.24×10^{-5}	CaV2	3.85	CaV3	0.001	0.23	40%
M6	0.0109	CaV1	2×10^{-7}	2×10^{-6}	8.24×10^{-5}	CaV2	3.85	CaV3	0.001	0.23	-9%
M7	0.0109	CaV1	2×10^{-6}	1×10^{-5}	8.24×10^{-5}	CaV2	3.85	CaV3	0.001	0.23	4%
M8	0.0109	CaV1	2×10^{-6}	2×10^{-7}	8.24×10^{-5}	CaV2	3.85	CaV3	0.001	0.23	-1%
M9	0.0109	CaV1	2×10^{-6}	2×10^{-6}	6.0×10^{-6}	CaV2	3.85	CaV3	0.001	0.23	-25%
M10	0.0109	CaV1	2×10^{-6}	2×10^{-6}	3.7×10^{-4}	CaV2	3.85	CaV3	0.001	0.23	95%
M11	0.0109	CaV1	2×10^{-6}	2×10^{-6}	8.24×10^{-5}	CaV2×0.1	3.85	CaV3	0.001	0.23	-1%

M12	0.0109	CaV1	2×10^{-6}	2×10^{-6}	8.24×10^{-5}	CaV2×10	3.85	CaV3	0.001	0.23	9%
M13	0.0109	CaV1	2×10^{-6}	2×10^{-6}	8.24×10^{-5}	CaV2	1	CaV3	0.001	0.23	-7%
M14	0.0109	CaV1	2×10^{-6}	2×10^{-6}	8.24×10^{-5}	CaV2	2.2	CaV3	0.001	0.23	-4%
M15	0.0109	CaV1	2×10^{-6}	2×10^{-6}	8.24×10^{-5}	CaV2	3.85	CaV3×0.1	0.001	0.23	-1%
M16	0.0109	CaV1	2×10^{-6}	2×10^{-6}	8.24×10^{-5}	CaV2	3.85	CaV3×10	0.001	0.23	4%
M17	0.0109	CaV1	2×10^{-6}	2×10^{-6}	8.24×10^{-5}	CaV2	3.85	CaV3	0.00077	0.23	1%
M18	0.0109	CaV1	2×10^{-6}	2×10^{-6}	8.24×10^{-5}	CaV2	3.85	CaV3	0.025	0.23	-24%
M19	0.0109	CaV1	2×10^{-6}	2×10^{-6}	8.24×10^{-5}	CaV2	3.85	CaV3	0.001	0.1	12%
M20	0.0109	CaV1	2×10^{-6}	2×10^{-6}	8.24×10^{-5}	CaV2	3.85	CaV3	0.001	0.44	-19%

The source of HONO is affected by many factors, and its concentration varies with any one of these factors. The sensitivity here is calculated by univariate analysis, that is, observing the changes in HONO concentration by changing only one variable but with all other variables unchanged. Here CaV1[a], CaV2[b] and CaV3[c] represented the Calculated values of OH (according to Eq. (8)), *As* is the surface area concentration of aerosol and $F_{HONO,soil}$ is soil emission flux (Oswald et al., 2013). The emission factor and δ are based on measurements in our previous work (Liu et al., 2020b). J_{NO3^-} (Liu et al., 2020a),V_d (Han et al., 2017) and $K_{dilution}$ (Dillon et al., 2002) are from references, respectively. The γ_{NO2} for aerosol and ground surface are calculated using Eq. (3-7). M0 represents the parameterized scheme input for the base case. M1-M20 are sensitivity analyses for different parameters in the HONO budget analysis, respectively.

Table S4. Periods and mean values (mean ± standard deviation, (minimum to maximum value)) of wind speed, $PM_{2.5}$, RH, T, HONO, trace gas, and NR-$PM_{2.5}$ in field observation.

Category	BCNY	COVID
Periods	January 1 - January 24	January 25 - March 6
Wind speed (m/s)	0.64±0.42 (0.04-3.65)	0.80±0.55 (0.02-3.86)
$PM_{2.5}$ (μg/m^3)	47.23±44.50 (3-265)	69.86±67.26 (2-268)
RH (%)	36.79±14.66 (12-94)	45.14±21.20 (12-95)
T (℃)	0.89±2.98 (-7.5–9.9)	3.42±3.97 (-6.8-12.6)
HONO (ppb)	0.97±0.74 (0.17-3.85)	0.53±0.45 (0.01-2.11)
NO (ppb)	18.42±29.24 (0.03-162.92)	2.44±5.40 (0.01-51.08)
NO_2 (ppb)	26.99±13.41 (2.68-54.51)	17.26±11.34 (0.57-64.44)
NO_X (ppb)	45.35±38.90 (2.27-207.46)	19.52±14.41 (0.33-89.09)
CO (ppb)	907.72±499.16 (294.93-3013.30)	954.87±624.04 (242.24-3751.68)
SO_2 (ppb)	2.09±1.36 (0.03-8.56)	1.47±1.95 (0.01-14.25)
O_3 (ppb)	12.16±10.79 (0.38-37.90)	21.29±11.78 (0.56-60.69)
NO_3^- (μg/m^3)	9.99±9.72 (0.09-57.62)	16.71±18.20 (0.08-89.28)
SO_4^{2-} (μg/m^3)	4.59±7.08 (0.43-56.91)	7.99±8.61 (0.35-37.39)
NH_4^+ (μg/m^3)	4.95±5.08 (0.23-31.90)	9.24±10.32 (0.17-51.36)
Cl^- (μg/m^3)	1.22±1.24 (0.01-6.72)	1.42±1.53 (0.01-8.37)
OA (μg/m^3)	14.71±10.75 (0.88-60.54)	18.19±16.52 (0.88-77.28)

Table S5. RF model performance for testing data set (in hourly time resolution).

Pollutants	RMSE	R	FAC2	MB	MGE	NMB	NMGE
HONO	0.21	0.93	0.86	0.01	0.15	0.02	0.21
NO	7.30	0.93	0.34	-0.21	3.76	-0.03	0.50
NO_2	4.38	0.94	0.93	-0.04	3.12	0.00	0.16
O_3	4.04	0.95	0.84	0.12	2.91	0.01	0.16
SO_2	0.63	0.93	0.68	0.01	0.38	0.01	0.27
CO	164.55	0.96	1.00	4.22	114.60	0.00	0.13
$PM_{2.5}$	12.88	0.98	0.88	0.83	8.70	0.01	0.15

Note: FAC2 (fraction of predictions with a factor of two), MB (mean bias), MGE (mean gross error), NMB (normalized mean bias), NMGE (normalized mean gross error), COE (Coefficient of Efficiency), IOA (Index of Agreement).

Table S6. Periods and concentration after deweather (mean ± standard deviation) of $PM_{2.5}$, HONO, trace gases in field observation, and the percentages in parentheses are concentration changes after deweather. Relative change in observed values and deweather values in different periods.

Category	BCNY (1.1-1.24)		COVID (1.25-3.6)		Relative change	
	Deweather	Observed	Deweather	Observed	Deweather	Observed
$PM_{2.5}$ ($\mu g/m^3$)	45.22±28.56 (-4.3%)	47.23±44.50	67.92±57.97 (-2.3%)	69.86±67.26	+50.2%	+47.9%
HONO (ppb)	0.89±0.37 (-8.3%)	0.97±0.74	0.51±0.25 (-3.8%)	0.53±0.45	-42.7%	-45.4%
NO (ppb)	15.44±18.40 (-16.2%)	18.42±29.24	3.24±2.05 (+32.8%)	2.44±5.40	-79.0%	-86.8%
NO_2 (ppb)	23.28±7.28 (-13.8%)	26.99±13.41	16.43±5.98 (-4.8%)	17.26±11.34	-29.4%	-36.1%
CO (ppb)	823.60±318.92 (-9.3%)	907.72±499.16	896±488.29 (-6.2%)	954.87±624.04	+8.8%	+5.2%
SO_2 (ppb)	2.27±0.69 (+8.6%)	2.09±1.36	1.48±1.18 (+0.7%)	1.47±1.95	-34.8%	+29.7%
O_3 (ppb)	16.98±5.62 (+39.6%)	12.16±10.79	22.60±4.10 (+6.2%)	21.29±11.78	+33.1%	+75.1%

Table S7. Summaries for HONO concentration of field observation.

Location	Date	HONO	NO_2	NO	$PM_{2.5}$
This study	2020.1.1-2020.1.24	0.97±0.74	26.9±13.41	18.4±29.24	47.2±44.5
	2020.1.25-2020.3.6	0.53±0.44	17.2±11.34	2.43±5.39	69.9±67.2
Shijia Zhuang (Liu et al., 2020a)	2019.12.15-2020.1.22	2.43±1.08	31.7	26.3±26.2	137.9±85.8
Beijing (Liu et al., 2020b)	2018.2.1-2018.6.30	1.26±1.06			
Guangzhou (Li et al., 2012)	2006.7.3-2006.7.31	0.95(night) 0.24(day)	16.5(night) 4.5(day)		
Beijing (Spataro et al., 2013)	2007.1.23-2007.2.14	1.04±0.73	38.76±10.02		
	2007.8.2-2007.8.31	1.45±0.58	31.7±7.82		70.12±29.62
Hyytiälä.Finland (Oswald et al., 2015)	2010.7.12-2010.8.12	0.037(night) 0.027(day)			
Beijing (Tong et al., 2015)	2014.10.28-2014.12.2	1.45	37.4	44.4	
Hong Kong (Xu et al., 2015)	2011.8(Summer)	0.65	19.8	8	
	2011.11(Autumn)	0.93	26.8	10.1	
	2012.2(Winter)	0.91	24.7	19.3	

	2012.5(Spring)	0.35	15.5	5.5	
Beijing (Tong et al., 2016)	2015.12.12-2015.12.22	1.34(haze) 0.51(clean)	28.4(haze) 7.1(clean)	70.73(haze) 17.0(clean)	144 (haze) 29 (clean)
Xi'an (Huang et al., 2017)	2015.7.24-2015.8.6	1.12±0.97	20.9±11.0		
Beijing (Wang et al., 2017)	2015.9.22-10.21(Autumn)	2.27±1.82	32.91±20.44	38.79(night)	99.28(night)
	2016.1.3-1.27(Winter)	1.05±0.89	19.96±16.28	65.65(night)	95.75(night)
	2016.4.1-5.14(Spring)	1.05±0.95	25.97±15.8	21.39(night)	56.6(night)
	2016.6.20-7.25(Summer)	1.38±0.9	19.21±11.25	3.08(night)	49.55(night)
Shanghai (Cui et al., 2018)	2016.5.12-2016.5.28	2.31	46.46		
Ji'nan (Li et al., 2018)	2015.9-2015.11(Autumn)	0.87±0.66	25.4±23.2	12.6	
	2015.12-2016.2(Winter)	2.15±1.35	41.1±34.6	37.4	
	2016.3-2016.5(Spring)	1.24±1.04	35.8±25.8	11.5	
	2016.6-2016.8(Summer)	1.2±1.01	22.5±19.0	6.6	
Nanjing (Liu et al., 2019a)	2017.12-2018.2(Winter)	1.15(night); 0.92(day)	28.4(night);23(day)	17.1(night);14.6(day)	
	2018.3-5 (Spring)	0.76(night);0.59 (day)	17.4(night);12.9(day)	1.7(night);3.0(day)	
	2018.6-8 (Summer)	0.56(night);0.34(day)	12.5(night);7.7(day)	1.0(night);1.4(day)	

	2018.9-11 (Autumn)	0.81(night);0.51(day)	18.9(night);13.4(day)	6.2(night);4.3(day)
Beijing (Zhang et al., 2019c)	2016.12	3.5±2.7	56±23	67±48
	2016.12(clean)	0.5 ± 0.2	19 ± 9	5 ± 5
	2016.12(haze)	3.4 ± 1.7	60 ± 13	75 ± 39
	2016.12(severe haze)	5.8 ± 3.0	76 ± 14	94 ± 40
Nanjing (Zheng et al., 2020)	2015.12.1-12.31	1.32±0.92	23.9±7.5	
Beijing (Liu et al., 2021)	2018.5.25-7.15(Summer)	1.27 ± 0.44	18.98 ± 4.47	
	2018.11.26-2019.1.15(winter)	1.13 ± 0.68	19.99 ± 9.38	
Xiamen (Hu et al., 2022)	2018.8 (Summer)	0.51(night);0.72(day)	15.7(night);11.0(day)	3.2(night);5.6(day)
	2018.10 (Autumn)	0.33(night);0.50(day)	14.3(night);11.4(day)	0.8(night);2.7(day)
	2018.12 (Winter)	0.52(night);0.61(day)	18.3(night);15.8(day)	4.8(night);12.2(day)
	2019.3 (Spring)	0.51(night);0.72(day)	17.7(night);18.5(day)	6.8(night);10.1(day)
Guangzhou (Yu et al., 2022)	2018.9-11	0.91(night);0.44(day)	36.9(night);23.3(day)	10.8(night);6.8(day)

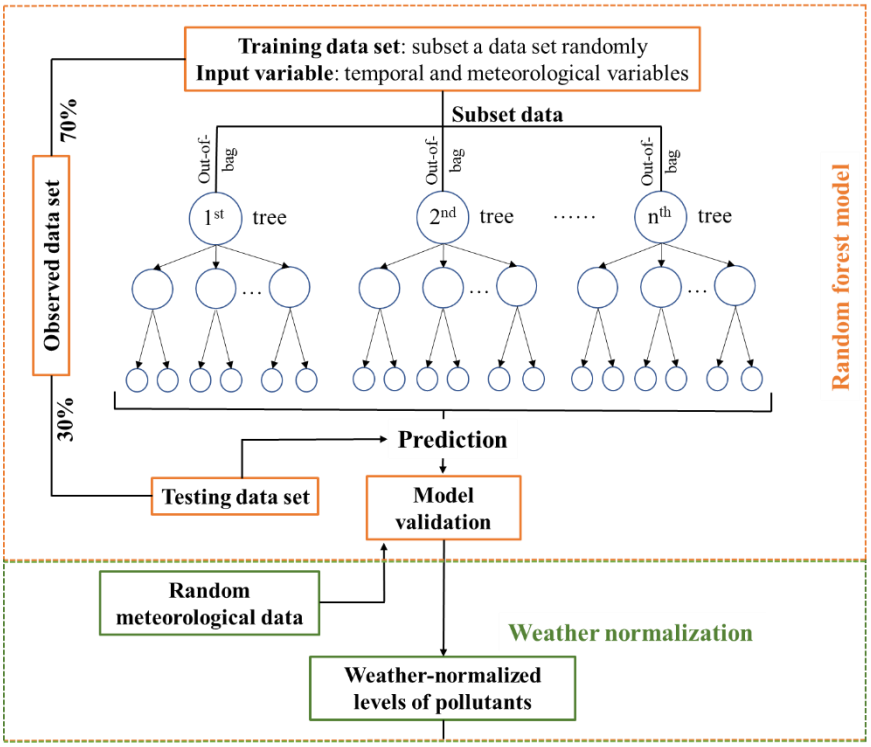

Fig. S1. The flowchart of the machine learning-based RF algorithm.

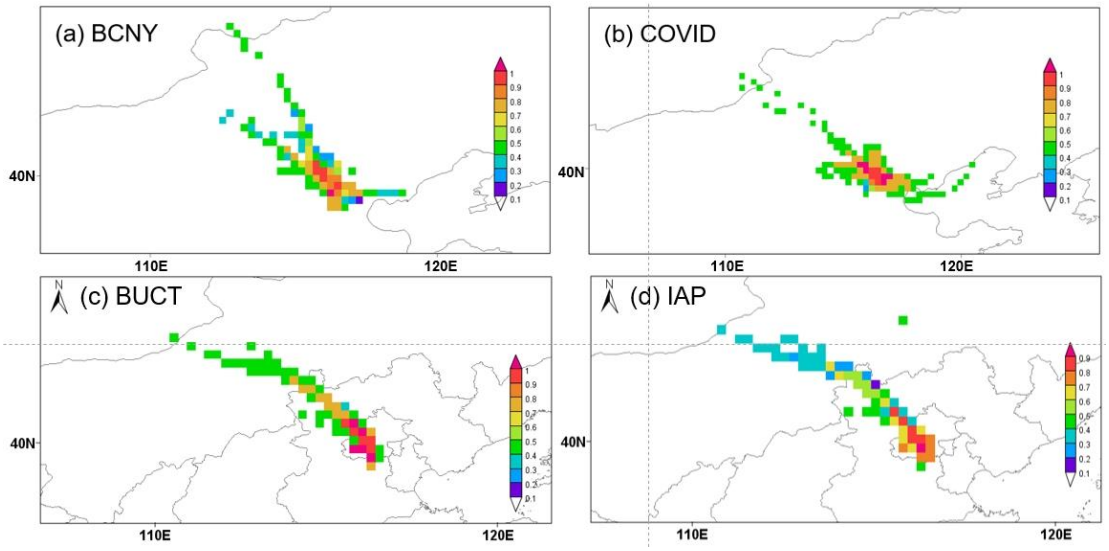

Figure S2. The potential source contribution function (PSCF) maps for the concentration of HONO (a and b are BCNY and COVID; c and d are BUCT and IAP stations, respectively). The comparison period of c and d is 2022.01.24-2022.01.31, and the trajectory of the air mass is 12 hours.

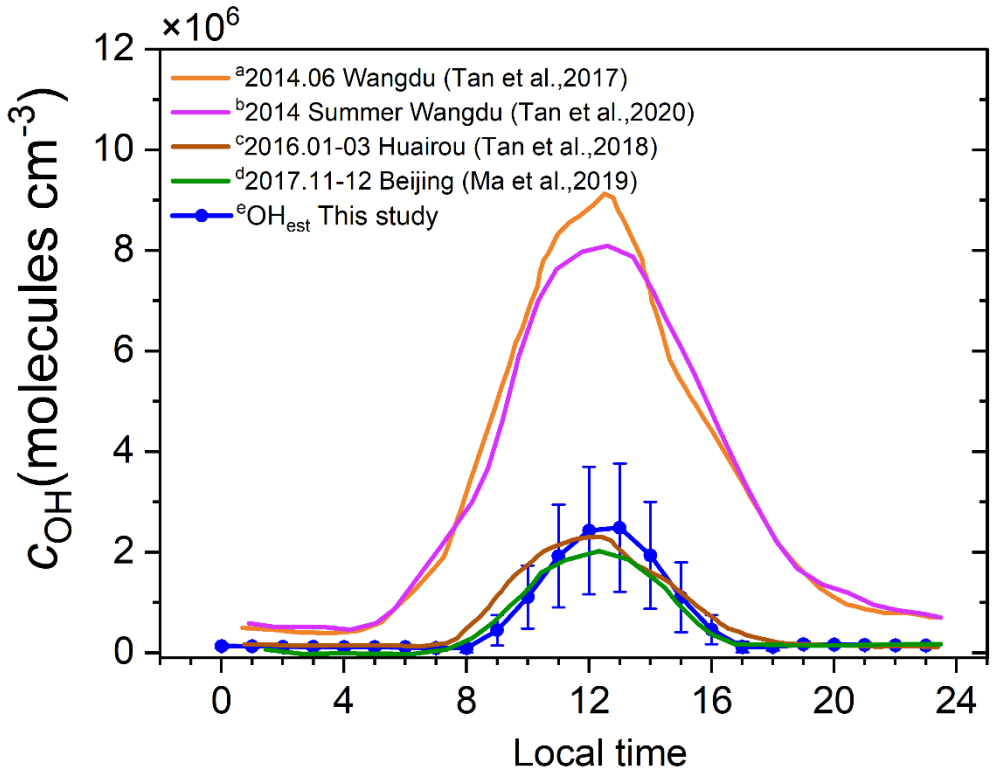

Figure S3. Diurnal variation of OH concentrations observed in different areas of the North China Plain (a-d) (Tan et al., 2017; Tan et al., 2018; Ma et al., 2019; Tan et al., 2020) and parameterized fitting in this study (e).

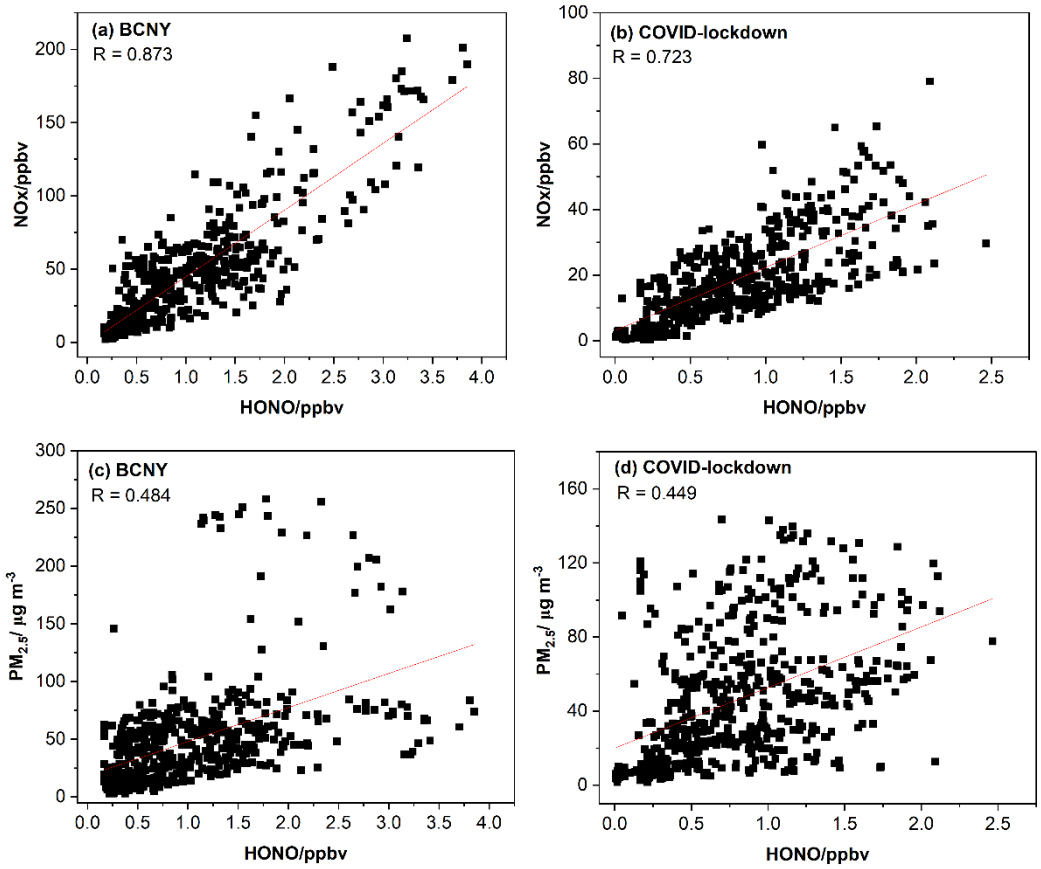

Figure S4. Correlation and scatterplot between HONO, NO_x (**a**: BCNY; **b**: COVID-lockdown) and $PM_{2.5}$ (**c**: BCNY; **d**: COVID-lockdown).

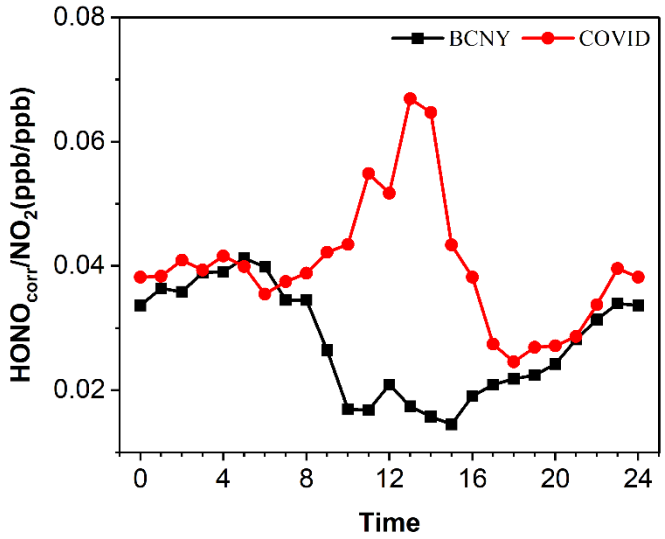

Figure S5. Diurnal variations of observed $HONO_{corr}/NO_2$ in BCNY (black line) and COVID (red line).

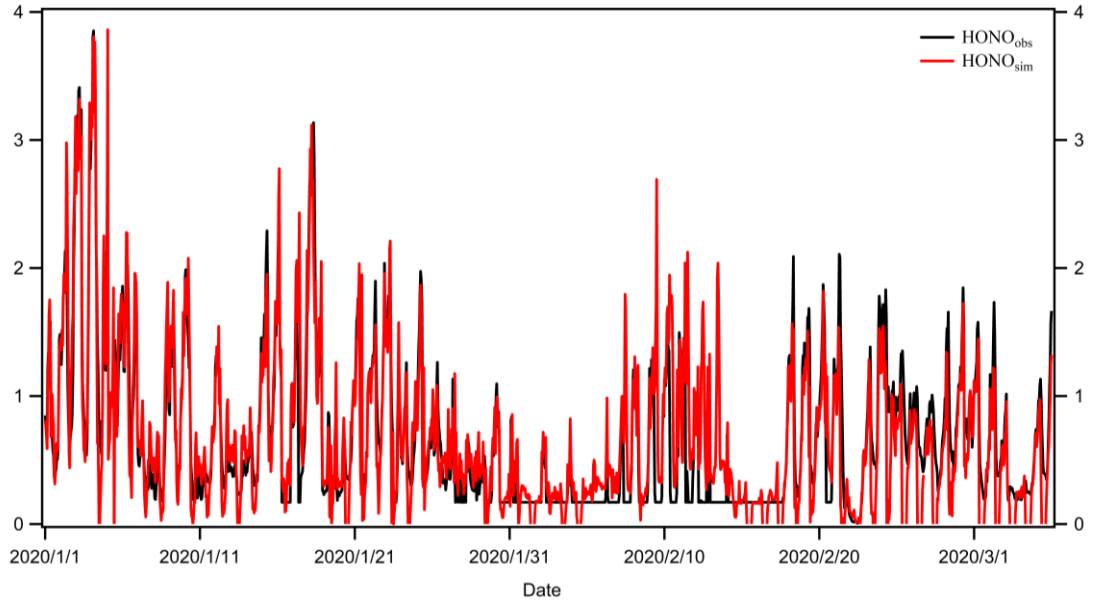

Figure S6. Comparison of simulated ($HONO_{sim}$, red line) and observed ($HONO_{obs}$, black line) hourly mean HONO concentration (ppbv) at the BUCT site over the period Jan. 1~Mar. 6, 2020.

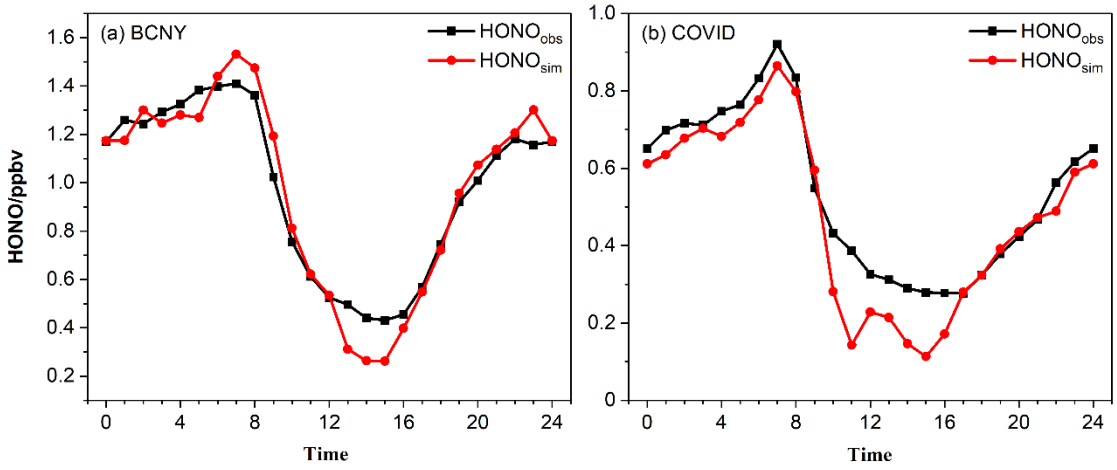

Figure S7. Observed and simulated HONO concentrations. Diurnal variations of observed HONO ($HONO_{obs}$, black line) and simulated HONO ($HONO_{sim}$, red line) in (**a**) BCNY and (**b**) COVID.

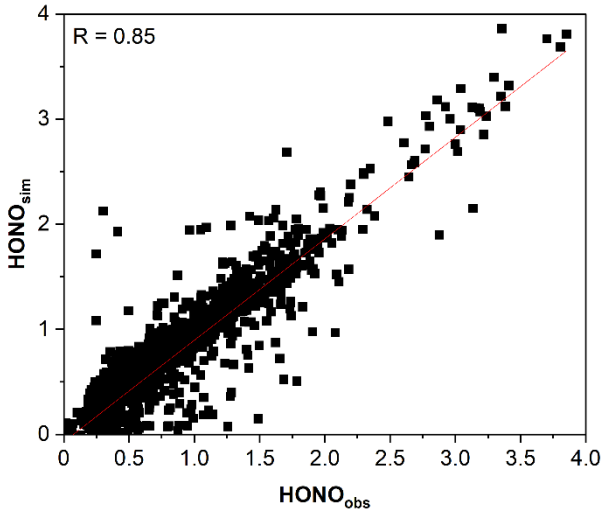

Figure S8. Correlation and Scatter plots between $HONO_{obs}$ and $HONO_{sim}$ (ppbv).

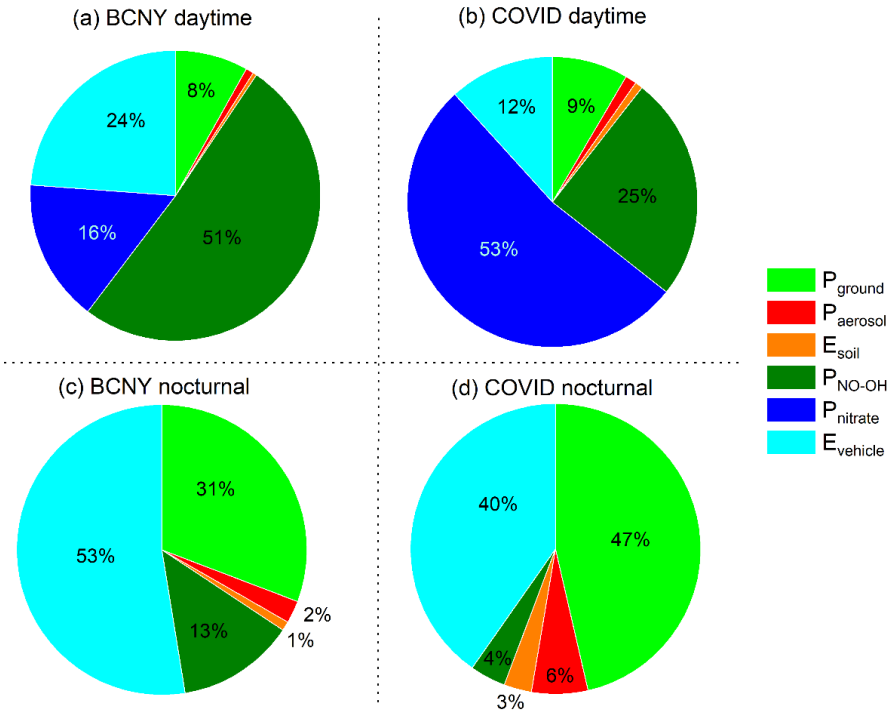

Figure S9. The percentage of daytime and nighttime contribution from different sources in (**a,c**) BCNY and (**b,d**) COVID. Pollutant concentrations are all raw concentrations.

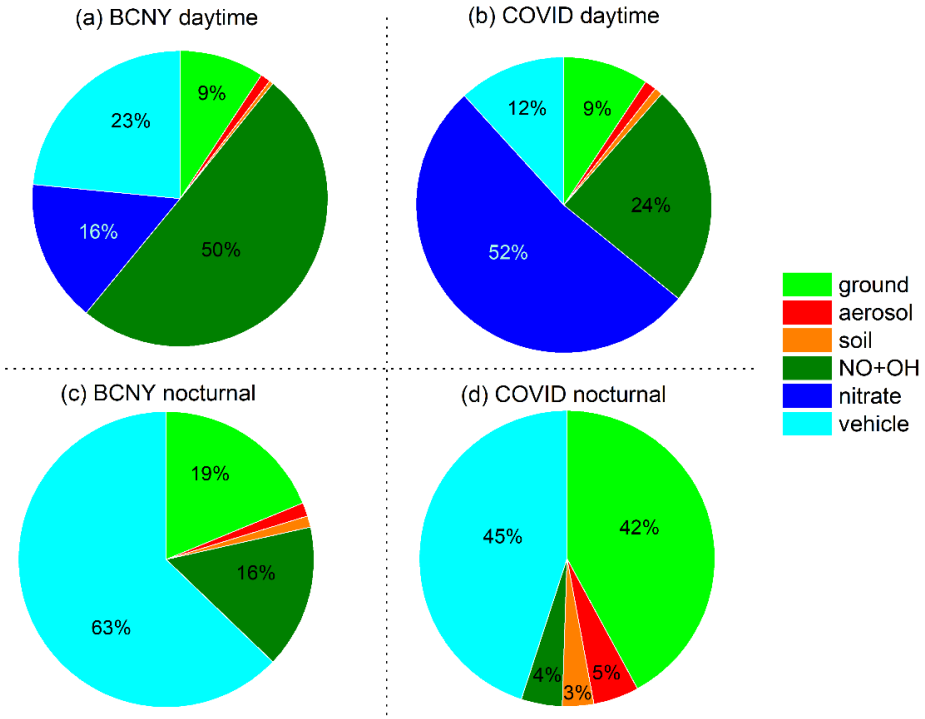

Figure S10. The percentage of daytime and nighttime contributions from different sources in (a,c) BCNY and (b,d) COVID. Pollutant concentrations are all de-weathering concentrations.

Reference

Bond, A. M. H., Frey, M. M., Kaiser, J., Kleffmann, J., Jones, A. E., and Squires, F. A.: Snowpack nitrate photolysis drives the summertime atmospheric nitrous acid (HONO) budget in coastal Antarctica, Atmospheric Chemistry and Physics, 23, 5533-5550, 10.5194/acp-23-5533-2023, 2023.

Breiman, L.: Random Forests, Machine Learning, 45, 5-32, https://doi.org/10.1023/A:1010933404324 2001.

Chai, J., Dibb, J. E., Anderson, B. E., Bekker, C., Blum, D. E., Heim, E., Jordan, C. E., Joyce, E. E., Kaspari, J. H., Munro, H., Walters, W. W., and Hastings, M. G.: Isotopic evidence for dominant secondary production of HONO in near-ground wildfire plumes, Atmospheric Chemistry and Physics, 21, 13077-13098, 10.5194/acp-21-13077-2021, 2021.

Cui, L., Li, R., Zhang, Y., Meng, Y., Fu, H., and Chen, J.: An observational study of nitrous acid (HONO) in Shanghai, China: The aerosol impact on HONO formation during the haze episodes, Sci Total Environ, 630, 1057-1070, 10.1016/j.scitotenv.2018.02.063, 2018.

Dillon, M. B., Lamanna, M. S., Schade, G. W., Goldstein, A. H., and Cohen, R. C.: Chemical evolution of the Sacramento urban plume: Transport and oxidation, Journal of Geophysical Research: Atmospheres, 107, ACH 3-1-ACH 3-15, 10.1029/2001jd000969, 2002.

Fu, X., Wang, T., Zhang, L., Li, Q., Wang, Z., Xia, M., Yun, H., Wang, W., Yu, C., Yue, D., Zhou, Y., Zheng, J., and Han, R.: The significant contribution of HONO to secondary pollutants during a severe winter pollution event in southern China, Atmospheric Chemistry and Physics, 19, 1-14, 10.5194/acp-19-1-2019, 2019.

Grange, S. K. and Carslaw, D. C.: Using meteorological normalisation to detect interventions in air quality time series, Sci Total Environ, 653, 578-588, 10.1016/j.scitotenv.2018.10.344, 2019.

Grange, S. K., Carslaw, D. C., Lewis, A. C., Boleti, E., and Hueglin, C.: Random forest meteorological normalisation models for Swiss PM_{10} trend analysis, Atmospheric Chemistry and Physics, 18, 6223-6239, 10.5194/acp-18-6223-2018, 2018.

Gu, R., Shen, H., Xue, L., Wang, T., Gao, J., Li, H., Liang, Y., Xia, M., Yu, C., Liu, Y., and Wang, W.: Investigating the sources of atmospheric nitrous acid (HONO) in the megacity of Beijing, China, Science of The Total Environment, 10.1016/j.scitotenv.2021.152270, 2021.

Han, X., Zhang, M., Skorokhod, A., and Kou, X.: Modeling dry deposition of reactive nitrogen in China with RAMS-CMAQ, Atmospheric Environment, 166, 47-61, 10.1016/j.atmosenv.2017.07.015, 2017.

Hu, B., Duan, J., Hong, Y., Xu, L., Li, M., Bian, Y., Qin, M., Fang, W., Xie, P., and Chen, J.: Exploration of the atmospheric chemistry of nitrous acid in a coastal city of southeastern China: results from measurements across four seasons, Atmospheric Chemistry and Physics, 22, 371-393, 10.5194/acp-22-371-2022, 2022.

Huang, R. J., Yang, L., Cao, J., Wang, Q., Tie, X., Ho, K. F., Shen, Z., Zhang, R., Li, G., Zhu, C., Zhang, N., Dai, W., Zhou, J., Liu, S., Chen, Y., Chen, J., and O'Dowd, C. D.: Concentration and sources of atmospheric nitrous acid (HONO) at an urban site in Western China, Sci Total Environ, 593-594, 165-172, 10.1016/j.scitotenv.2017.02.166, 2017.

Jia, C., Tong, S., Zhang, W., Zhang, X., Li, W., Wang, Z., Wang, L., Liu, Z., Hu, B., Zhao, P., and Ge, M.: Pollution characteristics and potential sources of nitrous acid (HONO) in early autumn 2018 of Beijing, Sci Total Environ, 735, 139317, 10.1016/j.scitotenv.2020.139317, 2020.

Kramer, L. J., Crilley, L. R., Adams, T. J., Ball, S. M., Pope, F. D., and Bloss, W. J.: Nitrous acid (HONO) emissions under real-world driving conditions from vehicles in a UK road tunnel, Atmospheric

Chemistry and Physics, 20, 5231-5248, 10.5194/acp-20-5231-2020, 2020.
Li, D., Xue, L., Wen, L., Wang, X., Chen, T., Mellouki, A., Chen, J., and Wang, W.: Characteristics and sources of nitrous acid in an urban atmosphere of northern China: Results from 1-yr continuous observations, Atmospheric Environment, 182, 296-306, 10.1016/j.atmosenv.2018.03.033, 2018.
Li, X., Brauers, T., Häseler, R., Bohn, B., Fuchs, H., Hofzumahaus, A., Holland, F., Lou, S., Lu, K. D., Rohrer, F., Hu, M., Zeng, L. M., Zhang, Y. H., Garland, R. M., Su, H., Nowak, A., Wiedensohler, A., Takegawa, N., Shao, M., and Wahner, A.: Exploring the atmospheric chemistry of nitrous acid (HONO) at a rural site in Southern China, Atmospheric Chemistry and Physics, 12, 1497-1513, 10.5194/acp-12-1497-2012, 2012.
Li, Y., Wang, X., Wu, Z., Li, L., Wang, C., Li, H., Zhang, X., Zhang, Y., Li, J., Gao, R., Xue, L., Mellouki, A., Ren, Y., and Zhang, Q.: Atmospheric nitrous acid (HONO) in an alternate process of haze pollution and ozone pollution in urban Beijing in summertime: Variations, sources and contribution to atmospheric photochemistry, Atmospheric Research, 260, 10.1016/j.atmosres.2021.105689, 2021.
Liu, J., Liu, Z., Ma, Z., Yang, S., Yao, D., Zhao, S., Hu, B., Tang, G., Sun, J., Cheng, M., Xu, Z., and Wang, Y.: Detailed budget analysis of HONO in Beijing, China: Implication on atmosphere oxidation capacity in polluted megacity, Atmospheric Environment, 244, 10.1016/j.atmosenv.2020.117957, 2021.
Liu, Y., Nie, W., Xu, Z., Wang, T., Wang, R., Li, Y., Wang, L., Chi, X., and Ding, A.: Semi-quantitative understanding of source contribution to nitrous acid (HONO) based on 1 year of continuous observation at the SORPES station in eastern China, Atmospheric Chemistry and Physics, 19, 13289-13308, 10.5194/acp-19-13289-2019, 2019a.
Liu, Y., Ni, S., Jiang, T., Xing, S., Zhang, Y., Bao, X., Feng, Z., Fan, X., Zhang, L., and Feng, H.: Influence of Chinese New Year overlapping COVID-19 lockdown on HONO sources in Shijiazhuang, Sci Total Environ, 745, 141025, 10.1016/j.scitotenv.2020.141025, 2020a.
Liu, Y., Lu, K., Li, X., Dong, H., Tan, Z., Wang, H., Zou, Q., Wu, Y., Zeng, L., Hu, M., Min, K. E., Kecorius, S., Wiedensohler, A., and Zhang, Y.: A Comprehensive Model Test of the HONO Sources Constrained to Field Measurements at Rural North China Plain, Environ Sci Technol, 53, 3517-3525, 10.1021/acs.est.8b06367, 2019b.
Liu, Y., Zhang, Y., Lian, C., Yan, C., Feng, Z., Zheng, F., Fan, X., Chen, Y., Wang, W., Chu, B., Wang, Y., Cai, J., Du, W., Daellenbach, K. R., Kangasluoma, J., Bianchi, F., Kujansuu, J., Petäjä, T., Wang, X., Hu, B., Wang, Y., Ge, M., He, H., and Kulmala, M.: The promotion effect of nitrous acid on aerosol formation in wintertime in Beijing: the possible contribution of traffic-related emissions, Atmospheric Chemistry and Physics, 20, 13023-13040, 10.5194/acp-20-13023-2020, 2020b.
Ma, X., Tan, Z., Lu, K., Yang, X., Liu, Y., Li, S., Li, X., Chen, S., Novelli, A., Cho, C., Zeng, L., Wahner, A., and Zhang, Y.: Winter photochemistry in Beijing: Observation and model simulation of OH and HO2 radicals at an urban site, Sci Total Environ, 685, 85-95, 10.1016/j.scitotenv.2019.05.329, 2019.
Meng, F., Qin, M., Tang, K., Duan, J., Fang, W., Liang, S., Ye, K., Xie, P., Sun, Y., Xie, C., Ye, C., Fu, P., Liu, J., and Liu, W.: High-resolution vertical distribution and sources of HONO and NO2 in the nocturnal boundary layer in urban Beijing, China, Atmospheric Chemistry and Physics, 20, 5071-5092, 10.5194/acp-20-5071-2020, 2020.
Meusel, H., Tamm, A., Kuhn, U., Wu, D., Leifke, A. L., Fiedler, S., Ruckteschler, N., Yordanova, P., Lang-Yona, N., Pöhlker, M., Lelieveld, J., Hoffmann, T., Pöschl, U., Su, H., Weber, B., and Cheng, Y.: Emission of nitrous acid from soil and biological soil crusts represents an important source of HONO in the remote atmosphere in Cyprus, Atmospheric Chemistry and Physics, 18, 799-813, 10.5194/acp-18-799-2018, 2018.

Oswald, R., Behrendt, T., Ermel, M., Wu, D., Su, H., Cheng, Y., Breuninger, C., Moravek, A., Mougin, E., Delon, C., Loubet, B., Pommerening-Roser, A., Sorgel, M., Poschl, U., Hoffmann, T., Andreae, M. O., Meixner, F. X., and Trebs, I.: HONO emissions from soil bacteria as a major source of atmospheric reactive nitrogen, Science, 341, 1233-1235, 10.1126/science.1242266, 2013.

Oswald, R., Ermel, M., Hens, K., Novelli, A., Ouwersloot, H. G., Paasonen, P., Petäjä, T., Sipilä, M., Keronen, P., Bäck, J., Königstedt, R., Hosaynali Beygi, Z., Fischer, H., Bohn, B., Kubistin, D., Harder, H., Martinez, M., Williams, J., Hoffmann, T., Trebs, I., and Sörgel, M.: A comparison of HONO budgets for two measurement heights at a field station within the boreal forest in Finland, Atmospheric Chemistry and Physics, 15, 799-813, 10.5194/acp-15-799-2015, 2015.

Ren, Y., Stieger, B., Spindler, G., Grosselin, B., Mellouki, A., Tuch, T., Wiedensohler, A., and Herrmann, H.: Role of the dew water on the ground surface in HONO distribution: a case measurement in Melpitz, Atmospheric Chemistry and Physics, 20, 13069-13089, 10.5194/acp-20-13069-2020, 2020.

Shetter, R. E., Junkermann, W., Swartz, W. H., Frost, G. J., Crawford, J. H., Lefer, B. L., Barrick, J. D., Hall, S. R., Hofzumahaus, A., Bais, A., Calvert, J. G., Cantrell, C. A., Madronich, S., Müller, M., Kraus, A., Monks, P. S., Edwards, G. D., McKenzie, R., Johnston, P., Schmitt, R., Griffioen, E., Krol, M., Kylling, A., Dickerson, R. R., Lloyd, S. A., Martin, T., Gardiner, B., Mayer, B., Pfister, G., Röth, E. P., Koepke, P., Ruggaber, A., Schwander, H., and van Weele, M.: Photolysis frequency of NO2: Measurement and modeling during the International Photolysis Frequency Measurement and Modeling Intercomparison (IPMMI), Journal of Geophysical Research: Atmospheres, 108, 10.1029/2002jd002932, 2003.

Shi, X., Ge, Y., Zheng, J., Ma, Y., Ren, X., and Zhang, Y.: Budget of nitrous acid and its impacts on atmospheric oxidative capacity at an urban site in the central Yangtze River Delta region of China, Atmospheric Environment, 238, 10.1016/j.atmosenv.2020.117725, 2020.

Song, Y., Zhang, Y., Xue, C., Liu, P., He, X., Li, X., and Mu, Y.: The seasonal variations and potential sources of nitrous acid (HONO) in the rural North China Plain, Environ Pollut, 311, 119967, 10.1016/j.envpol.2022.119967, 2022.

Spataro, F., Ianniello, A., Esposito, G., Allegrini, I., Zhu, T., and Hu, M.: Occurrence of atmospheric nitrous acid in the urban area of Beijing (China), Science of The Total Environment, 447, 210-224, 10.1016/j.scitotenv.2012.12.065, 2013.

Tan, Z., Hofzumahaus, A., Lu, K., Brown, S. S., Holland, F., Huey, L. G., Kiendler-Scharr, A., Li, X., Liu, X., Ma, N., Min, K. E., Rohrer, F., Shao, M., Wahner, A., Wang, Y., Wiedensohler, A., Wu, Y., Wu, Z., Zeng, L., Zhang, Y., and Fuchs, H.: No Evidence for a Significant Impact of Heterogeneous Chemistry on Radical Concentrations in the North China Plain in Summer 2014, Environ Sci Technol, 54, 5973-5979, 10.1021/acs.est.0c00525, 2020.

Tan, Z., Fuchs, H., Lu, K., Hofzumahaus, A., Bohn, B., Broch, S., Dong, H., Gomm, S., Häseler, R., He, L., Holland, F., Li, X., Liu, Y., Lu, S., Rohrer, F., Shao, M., Wang, B., Wang, M., Wu, Y., Zeng, L., Zhang, Y., Wahner, A., and Zhang, Y.: Radical chemistry at a rural site (Wangdu) in the North China Plain: observation and model calculations of OH, HO2 and RO2 radicals, Atmospheric Chemistry and Physics, 17, 663-690, 10.5194/acp-17-663-2017, 2017.

Tan, Z., Rohrer, F., Lu, K., Ma, X., Bohn, B., Broch, S., Dong, H., Fuchs, H., Gkatzelis, G. I., Hofzumahaus, A., Holland, F., Li, X., Liu, Y., Liu, Y., Novelli, A., Shao, M., Wang, H., Wu, Y., Zeng, L., Hu, M., Kiendler-Scharr, A., Wahner, A., and Zhang, Y.: Wintertime photochemistry in Beijing: observations of ROx radical concentrations in the North China Plain during the BEST-ONE campaign, Atmospheric Chemistry and Physics, 18, 12391-12411, 10.5194/acp-18-12391-2018, 2018.

Tang, M.-X., He, L.-Y., Xia, S.-Y., Jiang, Z., He, D.-Y., Guo, S., Hu, R.-Z., Zeng, H., and Huang, X.-F.: Coarse particles compensate for missing daytime sources of nitrous acid and enhance atmospheric oxidation capacity in a coastal atmosphere, Science of The Total Environment, 915, 10.1016/j.scitotenv.2024.170037, 2024.

Tong, S., Hou, S., Zhang, Y., Chu, B., Liu, Y., He, H., Zhao, P., and Ge, M.: Comparisons of measured nitrous acid (HONO) concentrations in a pollution period at urban and suburban Beijing, in autumn of 2014, Science China Chemistry, 58, 1393-1402, 10.1007/s11426-015-5454-2, 2015.

Tong, S., Hou, S., Zhang, Y., Chu, B., Liu, Y., He, H., Zhao, P., and Ge, M.: Exploring the nitrous acid (HONO) formation mechanism in winter Beijing: direct emissions and heterogeneous production in urban and suburban areas, Faraday Discuss, 189, 213-230, 10.1039/c5fd00163c, 2016.

Wang, J., Zhang, X., Guo, J., Wang, Z., and Zhang, M.: Observation of nitrous acid (HONO) in Beijing, China: Seasonal variation, nocturnal formation and daytime budget, Sci Total Environ, 587-588, 350-359, 10.1016/j.scitotenv.2017.02.159, 2017.

Xing, C., Xu, S., Song, Y., Liu, C., Liu, Y., Lu, K., Tan, W., Zhang, C., Hu, Q., Wang, S., Wu, H., and Lin, H.: A new insight into the vertical differences in NO2 heterogeneous reaction to produce HONO over inland and marginal seas, Atmospheric Chemistry and Physics, 23, 5815-5834, 10.5194/acp-23-5815-2023, 2023.

Xu, Z., Wang, T., Wu, J., Xue, L., Chan, J., Zha, Q., Zhou, S., Louie, P. K. K., and Luk, C. W. Y.: Nitrous acid (HONO) in a polluted subtropical atmosphere: Seasonal variability, direct vehicle emissions and heterogeneous production at ground surface, Atmospheric Environment, 106, 100-109, 10.1016/j.atmosenv.2015.01.061, 2015.

Xue, C., Zhang, C., Ye, C., Liu, P., Catoire, V., Krysztofiak, G., Chen, H., Ren, Y., Zhao, X., Wang, J., Zhang, F., Zhang, C., Zhang, J., An, J., Wang, T., Chen, J., Kleffmann, J., Mellouki, A., and Mu, Y.: HONO Budget and Its Role in Nitrate Formation in the Rural North China Plain, Environmental Science & Technology, 54, 11048-11057, 10.1021/acs.est.0c01832, 2020.

Ye, C., Lu, K., Ma, X., Qiu, W., Li, S., Yang, X., Xue, C., Zhai, T., Liu, Y., Li, X., Li, Y., Wang, H., Tan, Z., Chen, X., Dong, H., Zeng, L., Hu, M., and Zhang, Y.: HONO chemistry at a suburban site during the EXPLORE-YRD campaign in 2018: formation mechanisms and impacts on O3 production, Atmospheric Chemistry and Physics, 23, 15455-15472, 10.5194/acp-23-15455-2023, 2023.

Yu, Y., Cheng, P., Li, H., Yang, W., Han, B., Song, W., Hu, W., Wang, X., Yuan, B., Shao, M., Huang, Z., Li, Z., Zheng, J., Wang, H., and Yu, X.: Budget of nitrous acid (HONO) at an urban site in the fall season of Guangzhou, China, Atmospheric Chemistry and Physics, 22, 8951-8971, 10.5194/acp-22-8951-2022, 2022.

Zhan, Y., Luo, Y., Deng, X., Zhang, K., Zhang, M., Grieneisen, M. L., and Di, B.: Satellite-Based Estimates of Daily NO(2) Exposure in China Using Hybrid Random Forest and Spatiotemporal Kriging Model, Environ Sci Technol, 52, 4180-4189, 10.1021/acs.est.7b05669, 2018.

Zhang, J., An, J., Qu, Y., Liu, X., and Chen, Y.: Impacts of potential HONO sources on the concentrations of oxidants and secondary organic aerosols in the Beijing-Tianjin-Hebei region of China, Sci Total Environ, 647, 836-852, 10.1016/j.scitotenv.2018.08.030, 2019a.

Zhang, J., Chen, J., Xue, C., Chen, H., Zhang, Q., Liu, X., Mu, Y., Guo, Y., Wang, D., Chen, Y., Li, J., Qu, Y., and An, J.: Impacts of six potential HONO sources on HOx budgets and SOA formation during a wintertime heavy haze period in the North China Plain, Sci Total Environ, 681, 110-123, 10.1016/j.scitotenv.2019.05.100, 2019b.

Zhang, L., Wang, T., Zhang, Q., Zheng, J., Xu, Z., and Lv, M.: Potential sources of nitrous acid (HONO)

and their impacts on ozone: A WRF-Chem study in a polluted subtropical region, Journal of Geophysical Research: Atmospheres, 121, 3645-3662, 10.1002/2015jd024468, 2016.
Zhang, Q., Liu, P., George, C., Chen, T., Ren, Y., Mu, Y., Song, M., Herrmann, H., Mellouki, A., Chen, J., Zhao, X., and Zeng, Y.: Unveiling the underestimated direct emissions of nitrous acid (HONO), Proceedings of the National Academy of Sciences, 120, 10.1073/pnas, 2023.
Zhang, W., Tong, S., Ge, M., An, J., Shi, Z., Hou, S., Xia, K., Qu, Y., Zhang, H., Chu, B., Sun, Y., and He, H.: Variations and sources of nitrous acid (HONO) during a severe pollution episode in Beijing in winter 2016, Sci Total Environ, 648, 253-262, 10.1016/j.scitotenv.2018.08.133, 2019c.
Zhang, W., Tong, S., Jia, C., Wang, L., Liu, B., Tang, G., Ji, D., Hu, B., Liu, Z., Li, W., Wang, Z., Liu, Y., Wang, Y., and Ge, M.: Different HONO Sources for Three Layers at the Urban Area of Beijing, Environ Sci Technol, 54, 12870-12880, 10.1021/acs.est.0c02146, 2020.
Zhang, X., Tong, S., Jia, C., Zhang, W., Li, J., Wang, W., Sun, Y., Wang, X., Wang, L., Ji, D., Wang, L., Zhao, P., Tang, G., Xin, J., Li, A., and Ge, M.: The Levels and Sources of Nitrous Acid (HONO) in Winter of Beijing and Sanmenxia, Journal of Geophysical Research: Atmospheres, 127, 10.1029/2021jd036278, 2022.
Zheng, J., Shi, X., Ma, Y., Ren, X., Jabbour, H., Diao, Y., Wang, W., Ge, Y., Zhang, Y., and Zhu, W.: Contribution of nitrous acid to the atmospheric oxidation capacity in an industrial zone in the Yangtze River Delta region of China, Atmospheric Chemistry and Physics, 20, 5457-5475, 10.5194/acp-20-5457-2020, 2020.